JCTC Journal of Chemical Theory and Computation

Article

pubs.acs.org/JCTC

Extended Lagrangian Density Functional Tight-Binding Molecular Dynamics for Molecules and Solids

Bálint Aradi,*[,†] Anders M. N. Niklasson,[‡] and Thomas Frauenheim[†]

[†]Bremen Center for Computational Materials Science, University of Bremen, Am Fallturm 1, 28359 Bremen, Germany

[‡]Theoretical Division, Los Alamos National Laboratory, Los Alamos, New Mexico 87545, United States

ABSTRACT: A computationally fast quantum mechanical molecular dynamics scheme using an extended Lagrangian density functional tight-binding formulation has been developed and implemented in the DFTB+ electronic structure program package for simulations of solids and molecular systems. The scheme combines the computational speed of self-consistent density functional tight-binding theory with the efficiency and long-term accuracy of extended Lagrangian Born−Oppenheimer molecular dynamics. For systems without self-consistent charge instabilities, only a single diagonalization or construction of the single-particle density matrix is required in each time step. The molecular dynamics simulation scheme can be applied to a broad range of problems in materials science, chemistry, and biology.

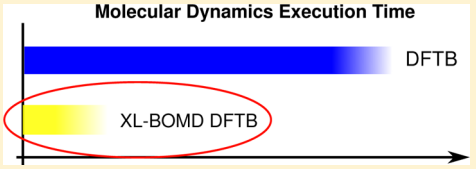

1. INTRODUCTION

Quantum-based molecular dynamics simulation methods, where the forces acting on the atoms are calculated on the fly using a quantum mechanical description of the electronic structure within the Born−Oppenheimer approximation, are becoming increasingly powerful for studies of solids and molecular systems.[1,2] Some early applications of Born−Oppenheimer molecular dynamics simulations date back 4 decades.[3,4] However, it was only after the development of the ingenious extended Lagranigan framework for density functional theory[5,6] by Car and Parrinello[7] that reliable first-principles molecular dynamics simulations with true predictive capability became widely avaliable.[1,2,8−10] A key advantage with Car and Parrinello's approach is that it avoids the self-consistent electronic ground state optimization that is required in regular Born−Oppenheimer molecular dynamics simulations. This provides a significant reduction of the computational cost. Car−Parrinello molecular dynamics also avoids some fundamental problems in regular Born−Oppenheimer molecular dynamics. In particular, a straightforward implementation of Born−Oppenheimer molecular dynamics is unstable and does not conserve energy without a high degree of convergence in the electronic structure calculations. If this is not achieved, then the electronic system behaves like a heat sink or source, gradually draining or adding energy to the atomic system due to a broken time reversibility.[8,11−14] Despite these shortcommings, regular Born−Oppenheimer molecular dynamics has become a workhorse for first-principles simulations. The reason is probably because of highly efficient software packages and the ability to use longer integration time steps. Shorter time steps are often necessary in Car−Parrinello simulations to avoid a nonadiabatic coupling between the nuclear and electronic degrees of freedom, in particular, in systems with a small electronic gap, which may significanlty increase the computational cost. Recently, an alternative approach based on an extended Lagrangian formulation of Born−Oppeheimer molecular dynamics was introduced, which avoids previous shortcomings and combines some of the best features of Car−Parrinello and regular Born−Oppenheimer molecular dynamics.[10,15−20] In this article, we present an extension of this approach to a computationally fast quantum mechanical molecular dynamics scheme using self-consistent density functional tight-binding theory (DFTB)[21−23] implemented in the DFTB+ electronic structure program package[24] for simulations of both solids and molecular systems. On the basis of the linearization of the DFTB total energy expression around auxiliary charges, the scheme combines the computational speed of DFTB with the efficiency and long-term stability of extended Lagrangian Born−Oppenheimer molecular dynamics.[15] For regular systems without self-consistent charge instabilities, only one diagonalization or construction of the single-particle density matrix is required in each time step. This is a significant improvement compared to an earlier DFTB implementation of extended Lagrangian Born−Oppenheimer molecular dynamics.[25] Our molecular dynamics DFTB+ implementation can be applied to a broad range of problems in materials science, chemistry, and biology.

The article is outlined as follows: First, we present extended Lagrangian Born−Oppenheimer molecular dynamics (XL-BOMD) and how it has been implemented in the DFTB+ program package. Thereafter, we show some examples by comparing it to a previous DFTB+ implementation of regular Born−Oppenheimer molecular dynamics. We demonstrate simulations both for solids and molecular systems. In the limit of only a single diagonalization or construction of the density matrix per time step, we also identify an important limitation, in particular for extended metallic systems, where

Received: April 7, 2015

DOI: 10.1021/acs.jctc.5b00324
J. Chem. Theory Comput. XXXX, XXX, XXX−XXX

instabilites in the self-consistent charge optimization may occur. At the end, we summarize the results and give our conclusions.

2. EXTENDED LAGRANGIAN BORN−OPPENHEIMER MOLECULAR DYNAMICS

Extended Lagrangian Born−Oppenheimer molecular dynamics[15] can be formulated in terms of a Lagrangian

$$\mathcal{L}^{\mathrm{XBO}}(\mathbf{R}, \dot{\mathbf{R}}, n, \dot{n}) = \frac{1}{2}\sum_I M_I\dot{R}_I^2 - U(\mathbf{R}; \rho(\mathbf{r})) + \frac{1}{2}\mu\int \dot{n}^2(\mathbf{r})\,\mathrm{d}\mathbf{r} - \frac{1}{2}\mu\omega^2\int (\rho(\mathbf{r}) - n(\mathbf{r}))^2\,\mathrm{d}\mathbf{r} \quad (1)$$

where the regular Born−Oppenheimer Lagrangian, which is defined at the relaxed electronic ground state density $\rho(\mathbf{r})$ for a given set of nuclear coordinates, $\{R_I\} = \mathbf{R}$, has been extended with auxiliary dynamical variables for the electronic degrees of freedom, $n(\mathbf{r})$ and $\dot{n}(\mathbf{r})$, that evolve in a harmonic well centered around $\rho(\mathbf{r})$. The dots denote the time derivatives. The potential energy $U(\mathbf{R}; \rho(\mathbf{r}))$ here is the Kohn−Sham energy functional including the ion−ion repulsion energy. The parameter μ is a fictitious electron mass, and ω is the frequency determining the curvature of the harmonic well. Euler−Lagrange equations, in the limit $\mu \to 0$,[15] give the decoupled equations of motion

$$M_I\ddot{R}_I = -\frac{\partial U(\mathbf{R}; \rho(\mathbf{r}))}{\partial R_I}\bigg|_n$$
$$\ddot{n}(\mathbf{r}) = \omega^2(\rho(\mathbf{r}) - n(\mathbf{r})) \quad (2)$$

The partial derivatives of U for the nuclear coordinates R_I are taken with respect to a constant auxiliary density $n(\mathbf{r})$, since $n(\mathbf{r})$ is an independent dynamical variable. The equations of motion can be integrated using time-reversible or symplectic schemes, for both the nuclear and electronic degrees of freedom.[26−30] By using a time-reversibly integrated density $n(\mathbf{r})$ from eq 2 as the initial guess of the iterative self-consistent field (SCF) optimization procedure

$$n(\mathrm{r}) \equiv n_0 \to n_1 \to \ldots \to n_\infty = \mathrm{SCF}(n_0) \equiv \rho(\mathrm{r}) \quad (3)$$

which requires one diagonalization and density construction per iteration, the total Born−Oppenheimer energy

$$E_{\mathrm{tot}}^{\mathrm{BO}} = \frac{1}{2}\sum_I M_I\dot{R}_I^2 + U(\mathbf{R}; \rho(\mathbf{r})) \quad (4)$$

remains stable without any long-term energy drift, even in the case of approximate convergence of $\rho(\mathbf{r})$.[15−17,31] This leads to a significant decrease of the computational cost while maintaining the long-term accuracy.

As a function of the number of SCF iterations in eq 3, we may use the notation $\rho_j(\mathbf{r}) \equiv \rho[n_j(\mathbf{r})]$ for the approximate ground state density, where

$$\rho(\mathbf{r}) = \lim_{j\to\infty} \rho[n_j(\mathbf{r})] \quad (5)$$

In the limit of only a single diagonalization and construction of the electron density per time step,[19,31] i.e., when $j = 0$, the equations of motion are given by

$$M_I\ddot{R}_I = -\frac{\partial U(\mathbf{R}; \rho[n(\mathbf{r})])}{\partial R_I}\bigg|_n$$
$$\ddot{n}(\mathbf{r}) = \omega^2(\rho[n(\mathbf{r})] - n(\mathbf{r})) \quad (6)$$

The simplicity of these equations of motion for an unoptimized and approximate ground state electron density can be deceptive, and great care is needed in the explicit formulation of the potential energy term $U(\mathbf{R}; \rho[n(\mathbf{r})])$ that no longer is uniquely defined beyond the exact ground state.[19,31,32] By choosing a particular linearized form of the electron−electron interaction, we get a potential energy that closely follows the exact Kohn−Sham ground state surface and that has a simple expression for the nuclear forces even if the Hellmann−Feynman ground state condition is not fullfilled.[20] We may view this modified potential as part of a shadow Hamiltonian. Thus, instead of integrating the equations of motion with approximately converged forces for an exact Kohn−Sham DFT dynamics, we integrate an approximate shadow dynamics with exact forces.[20] In this way, properties, such as the total energy or phase−space area, of an exact Hamiltonian dynamics can be rigorously controlled. This concept of backward analysis has previously been used in geometric integration schemes of classical Hamiltonian dynamics. Here, the same basic idea is applied to a potential energy surface that is generated from nonlinear self-consistent field theory. An alternative and more technical direct derivation of the equations of motion in the limit of only one diagonalization, eq 6, that more clearly shows the underlying assumptions is given in ref 20.

At finite electronic temperatures, the potential energy $U(\mathbf{R}; \rho[n(\mathbf{r})])$ is replaced by the free energy including the entropy contribution arising from the fractional occupation of the Kohn−Sham states,[33] and for nonorthogonal atomic orbital basis set representations, we also need to include a Pulay force.

The advantage with reaching an accurate dynamics already in the limit of vanishing SCF iterations is that it is also an ideal starting point for any subsequent improvements of the ground state toward an exact Born−Oppenheimer molecular dynamics. This will significantly reduce the computational cost. In fact, as we will demonstrate here, typically only a single diagonalization or construction of the density from the density matrix is required in each time step. This provides a significant speed up over regular Born−Oppenheimer molecular dynamics.

3. EXTENDED LAGRANGIAN DENSITY FUNCTIONAL TIGHT-BINDING MOLECULAR DYNAMICS

3.1. Equations of Motion for DFTB. In our particular implementation of extended Lagrangian Born−Oppenheimer molecular dynamics, we use the density functional tight-binding method in a restricted (non-spin-polarized) formulation that is described in refs 21, 23, and 24. In DFTB theory, the total energy is expanded usually up to second order in the density fluctuation $\delta\rho$ around a reference density ρ_0, which is the sum of neutral atomic densities. The total energy E_{tot} is then expressed as

$$E_{\mathrm{tot}} = E_{\mathrm{BS}}[\rho_0] + E_2[\rho_0, \delta\rho] + E_{\mathrm{rep}}[\rho_0] \quad (7)$$

as the sum of the band structure energy E_{BS}, the repulsive energy E_{rep}, and the second-order energy E_2. The first two terms are calculated explicitely with approximations, whereas the last one is fitted to ab initio DFT results or experiments, allowing DFTB to deliver accurate total energies despite its

DOI: 10.1021/acs.jctc.5b00324
J. Chem. Theory Comput. XXXX, XXX, XXX−XXX

approximations. Following the Kohn−Sham ansatz, the density is written as the sum of one-electron densities. The corresponding one-electron wave functions are expanded into a linear combination of atomic orbitals

$$\psi_i(\mathbf{r}) = \sum_\mu c_{\mu i}\phi_\mu(\mathbf{r}) \tag{8}$$

The coefficients and one-electron energies are determined by solving the generalized eigenvalue problem

$$\sum_\nu [H^0 + H^2]_{\mu\nu}c_{\nu i} = \epsilon_i \sum_\nu S_{\mu\nu}c_{\nu i} \tag{9}$$

where H^0 and H^2 are the Hamilton operators corresponding to the energy contributions E_{BS} and E_2, respectively, and S is the overlap matrix of the atomic orbitals. H^0 is calculated in a two-center-approximation, which simplifies its calculation to table lookups in precalculated integration tables. H^2 is derived from a point-charge-like model for the second-order energy

$$E_2 = \frac{1}{2}\sum_{\mu\nu}\gamma_{\mu\nu}\Delta q_\mu \Delta q_\nu \tag{10}$$

with the Mulliken net charges Δq_μ and Δq_ν on orbitals ϕ_μ and ϕ_ν, respectively, coupled with a Coulomb-like expression $\gamma_{\mu\nu}$ that also includes exchange-correlation effects. In the limit of only one diagonalization, where the construction of $\mathbf{q} = \{q_\mu\}$ is given in a single step from the auxiliary dynamical variable charges $\mathbf{n} = \{n_\mu\}$, we use a linearized expression, where

$$E_2 \approx \frac{1}{2}\sum_{\mu\nu}\gamma_{\mu\nu}(2\Delta q_\mu - \Delta n_\mu)\Delta n_\nu \tag{11}$$

The atomic Mulliken population for a given orbital ϕ_μ is obtained as

$$q_\mu = \frac{1}{2}\sum_\nu (P_{\mu\nu}S_{\nu\mu} + S_{\mu\nu}P_{\nu\mu}) \tag{12}$$

where $P_{\mu\nu}$ is the density matrix in the basis of the atomic orbitals

$$P_{\mu\nu} = \sum_i f_i c_{\mu i}c_{\nu i}^* \tag{13}$$

where the occupation number f_i takes values between 0 and 2 for spin unpolarized systems. The corresponding net charges Δq_μ and Δn_μ are given by subtracting the Mulliken charges of the neutral atoms.

Since the reference electron density ρ_0 is encoded in the precalculated integral tables and does not change during the dynamics, the Born−Oppenheimer energy for density functional based tight-binding molecular dynamics can be written as

$$E_{\mathrm{tot}}^{\mathrm{BO}} = \frac{1}{2}\sum_I M_I\dot{R}_I^2 + U(\mathbf{R};\,\mathbf{q}[\mathbf{n}]) \tag{14}$$

with

$$U(\mathbf{R};\,\mathbf{q}[\mathbf{n}]) = E_{\mathrm{BS}}(\mathbf{R}) + E_{\mathrm{rep}}(\mathbf{R}) + E_2(\mathbf{R};\,\mathbf{q}[\mathbf{n}]) \tag{15}$$

where the vector $\mathbf{q}[\mathbf{n}]$ contains the atomic Mulliken populations that have been calculated from the eigenstates of the Hamiltonian, $H[\mathbf{n}]$, determined for the auxiliary dynamical variable density $\mathbf{n}$. Accordingly, in the extended Lagrangian for DFTB, the charge densities $n(\mathbf{r})$ and $\rho[\mathbf{n}](\mathbf{r})$ in the limit of only one diagonalization in eq 2 are replaced by the corresponding Mulliken populations $\mathbf{n}$ and $\mathbf{q}$, leading to the XL-BOMD equations of motion

$$M_I\ddot{R}_I = -\left.\frac{\partial U(\mathbf{R};\,\mathbf{qn}])}{\partial R_I}\right|_{\mathbf{n}} \tag{16}$$

$$\ddot{\mathbf{n}} = \omega^2(\mathbf{q}[\mathbf{n}] - \mathbf{n}) \tag{17}$$

The partial derivatives in eq 16 are with respect to a constant dynamical variable density $\mathbf{n}(\mathbf{r})$. Because of an underlying nonorthogonal basis set used in DFTB, this expression also includes Pulay forces occurring from the derivatives of basis-set-dependent energy contributions. The force expression reads then as

$$M_I\ddot{R}_I = -\mathrm{Tr}\left[P\frac{\partial H^0}{\partial R_I}\right] - \frac{1}{2}\sum_{\mu,\nu}P_{\mu\nu}\left(\frac{\partial S}{\partial R_I}\right)_{\mu\nu}(V_\mu + V_\nu) - \frac{1}{2}\sum_{\mu,\nu}(2\Delta q_\mu - \Delta n_\mu)\Delta n_\nu\frac{\partial \gamma_{\mu\nu}}{\partial R_I} - \frac{\partial E_{\mathrm{rep}}}{\partial R_I} + \tilde{F}_I^P \tag{18}$$

with

$$V_\mu = \sum_\nu \gamma_{\mu\nu}\Delta n_\nu \tag{19}$$

being the total potential associated with all point-like net charges Δn_ν at the center of the atomic orbital μ. The term $\tilde{F}_I^P$ represents the Pulay force, which, in the limit of zero electronic temperature, can be calculated as

$$\tilde{F}_I^P = \mathrm{Tr}\left[PHP\frac{\partial S}{\partial R_I}\right] = \mathrm{Tr}\left[P(H^0 + H^2)P\frac{\partial S}{\partial R_I}\right] \tag{20}$$

where the Hamiltonian is calculated from the auxiliary dynamical variable density $\mathbf{n}$, i.e., $H^2 = H^2[\mathbf{n}]$. If multiple self-consistent charge iterations are used, then the auxiliary dynamical variable charges n_μ and Δn_μ are replaced by the updated ground state Mulliken charges q_μ and Δq_μ in the force and energy expressions.

3.2. Finite Electronic Temperatures. At finite electronic temperatures, $T_e > 0$, the potential energy $U(\mathbf{R};\,\mathbf{q}[\mathbf{n}])$ is replaced by the free energy term

$$\Omega(\mathbf{R};\,\mathbf{q}[\mathbf{n}],\,T_e) = U(\mathbf{R};\,\mathbf{q}[\mathbf{n}]) - T_e\mathcal{S} \tag{21}$$

where $\mathcal{S}$ is the entropy calculated from the fractional occupation, $\bar{\mathbf{f}} = \{\bar{f}_i\}$, of the Kohn−Sham orbitals

$$\mathcal{S} = -2k_B\sum_i \bar{f}_i\ln(\bar{f}_i) + (1 - \bar{f}_i)\ln(1 - \bar{f}_i) \tag{22}$$

The factor 2 is included since we have a restricted non-spin-polarized formulation, and the occupation numbers $\bar{f}_i$ take values between 0 and 1. For the variationally optimized free energy, the occupation factors are given from the Kohn−Sham eigenvalues, ε_i, by the Fermi−Dirac distribution

$$\bar{f}_i = [\exp(\beta(\varepsilon_i - \mu)) + 1]^{-1} \tag{23}$$

The entropy contribution is essential for variationally correct forces, and to provide a computationally tractable expression for the Pulay force, we use the form derived in ref 15, i.e.

$$\bar{F}_I^P = \frac{1}{2}\mathrm{Tr}\left[(PHS^{-1} + S^{-1}HP)\frac{\partial S}{\partial R_I}\right] \tag{24}$$

DOI: 10.1021/acs.jctc.5b00324
J. Chem. Theory Comput. XXXX, XXX, XXX−XXX

$$= \mathrm{Tr}\left[S^{-1}H[\mathbf{n}]\, P\frac{\partial S}{\partial R_I} \right] \tag{25}$$

3.3. Integration of Equations of Motion. To integrate the equations of motion for the nuclear degrees of freedom in eq 16, we use the regular velocity Verlet integration algorithm. For the integration of the electronic degrees of freedom in eq 17, we use the modified Verlet integration method described in ref 28, where

$$n_I(t+\delta t) = 2n_I(t) - n_I(t-\delta t) + \delta t^2 \ddot{n}_I(t) + \alpha \sum_{k=0}^{K} c_k n_I(t-k\delta t) \tag{26}$$

This Verlet scheme includes a weak dissipative force that avoids an accumulation of numerical noise present in any molecular dynamics simulation. If the numerical noise is not removed, then the auxiliary electronic degrees of freedom will eventually be distorted and no longer serve as an accurate guess to the exact ground state density. Optimized values of α, c_k, and the dimensionless variable $\kappa = \delta t^2\omega^2$ for various choices of the number of terms K in the dissipative force are given in Table 1.

Table 1. Optimized α and $\kappa = \delta t^2\omega^2$ Values and the c_k Coefficient for the Dissipative Electronic Force Term in eq 26[a]

K	κ	α	c_0	c_1	c_2	c_3	c_4	c_5	c_6	c_7
5	1.82	0.018	−6	14	−8	−3	4	−1		
6	1.84	0.0055	−14	36	−27	−2	12	−6	1	
7	1.86	0.0016	−36	99	−88	11	32	−25	8	−1

[a]See ref 28 for the derivation and a more complete set of coefficients and ref 25 for some evaluations.

To provide stability in the modified Verlet integration of the electronic degrees of freedom in eq 26 in the limit of vanishing SCF optimization, the parameter ω^2 in eq 17 or, alternatively, the dimensionless integration constant $\kappa = \delta t^2\omega^2$ that occurs in eq 26 typically needs to be rescaled by a κ-scaling factor $c \in [0, 1]$.[31] Stability can be only possibly guaranteed for convex energy functionals,[34] i.e., when there exists a constant $c \in [0, 1]$ such that

$$U[c\mathbf{q}(\mathbf{n}) + (1-c)\mathbf{n}] < cU[\mathbf{q}(\mathbf{n})] + (1-c)U[\mathbf{n}] \tag{27}$$

This requirement constrains the applicability of XL-BOMD in the limit of vanishing SCF optimization and an increased set of SCF iterations is required for nonconvex functionals. This is a particular problem for large extended metallic systems, where charge sloshing causes instabilities.

4. MOLECULAR DYNAMICS SIMULATIONS

In order to demonstrate its capabilities when coupled with the density functional tight-binding method, we have carried out extended Lagrangian Born−Oppenheimer molecular dynamics (XL-BOMD) simulations on various systems using the DFTB+ code.[24] In this section, we will compare the simulation results to conventional Born−Oppenheimer molecular dynamics (BOMD) simulations carried out with the same code. In order to follow the Born−Oppenheimer surface as close as possible, a very tight charge tolerance of 10^{-9} electrons had been chosen during the conventional BOMD simulations for the SCC convergence. The investigated systems had been first thermalized using a Nosé−Hoover chain[35] as the thermostat. After that, starting with the last coordinates and velocities of the thermalization process, separate BOMD and XL-BOMD simulations with constant volume and total energy (NVE) were carried out for 50 ps. The respective BOMD and XL-BOMD trajectories in those simulations are equivalent for the first 10 steps. During this phase, the integrator for the auxiliary charges in XL-BOMD was initialized with the values of the fully converged charges at each time step. In order to ensure a smooth transition, we have used a linear combination of the fully converged charges and the XL-BOMD predicted ones to fill the integrator for an additional 10 time steps. After that, the XL-BOMD simulations used only one diagonalization per time step, as described in the previous sections. For the dissipation term in eq 26, $K = 5$ was used in all simulations.

To demonstrate the similarities between regular BOMD and XL-BOMD trajectories, we have compared the evolution of the total energies with the time required for the first few picoseconds of the simulations. Due to the chaotic nature of molecular dynamics, longer comparisons of the details of the energy fluctuations are not meaningful. We have also calculated the velocity autocorrelation function $R(\tau)$ for each trajectory and Fourier transformed it to obtain the density of vibrational states. The velocity autocorrelation functions were, in all cases, calculated by averaging over the entire 50 ps MD trajectory with a correlation time window varying between 0 and 5 ps. Before the Fourier transformation, each autocorrelation function was multiplied by the Hann function and padded with zeros for an additional time period 10 times longer than the time window of the velocity−velocity autocorrelation function. We have finally taken the real component of the Fourier transform, which corresponds to a symmetrization of the velocity autocorrelation function in time, $R(\tau) = R(-\tau)$.

4.1. Molecules. As an example for molecular systems, we have chosen a liquid system of imidazol with 16 molecules in a supercell with periodic boundary conditions. The system was thermalized at 400 K, which is in between the melting and boiling points of the crystal. We have used the parametrization set `mio-1-1`[36] to describe the diatomic interactions in the system. The Brillouin-zone integration was done using the Γ-point approximation. We did not take the van der Waals interaction into account, as in DFTB it is usually realized via an empirical energy correction and, therefore, does not directly alter the electronic Hamiltonian or the charges, which are of relevance to the differences between regular BOMD and XL-BOMD. The κ-scaling factor c (as in eq 27) was chosen to be 0.5 during the XL-BOMD simulations. The size of the integration time step δt was chosen as 0.5 fs in all imidazol simulations.

We have tested two different electronic temperature settings: 0 K (no electron smearing) and 300 K. The two cases require different evaluations of the Pulay forces, as shown in eqs 20 and 24. The comparison of the XL-BOMD and BOMD total energy fluctuations as a function of time are shown in Figures 1 and 2 for the first 2 ps, respectively. The BOMD and XL-BOMD energy curves run close to each other, although the amplitude of the fluctuations is somewhat higher for the latter. The vibrational density of states, shown in the same figures, are practically identical.

4.2. Solids. The dynamics of solids is more challenging for the XL-BOMD method than it is for molecular systems, as, due to the compactness of a solid and the largely delocalized valence orbitals, even small deviances in the atomic charges can

DOI: 10.1021/acs.jctc.5b00324
J. Chem. Theory Comput. XXXX, XXX, XXX−XXX

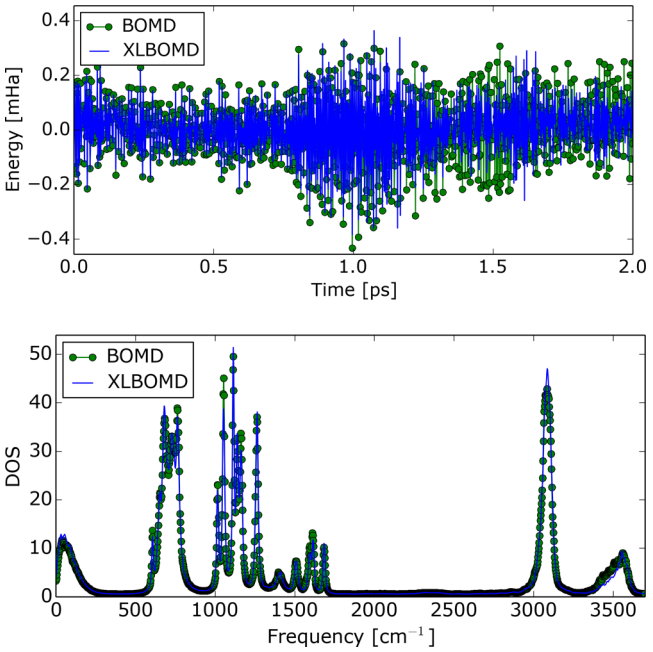

Figure 1. Total energy fluctuation (top) and vibrational density of states (bottom) for the imidazol crystal with 16 imidazol molecules using zero electronic and 400 K ionic temperature. Green dots and blue lines represent the results of the BOMD and XL-BOMD simulations, respectively.

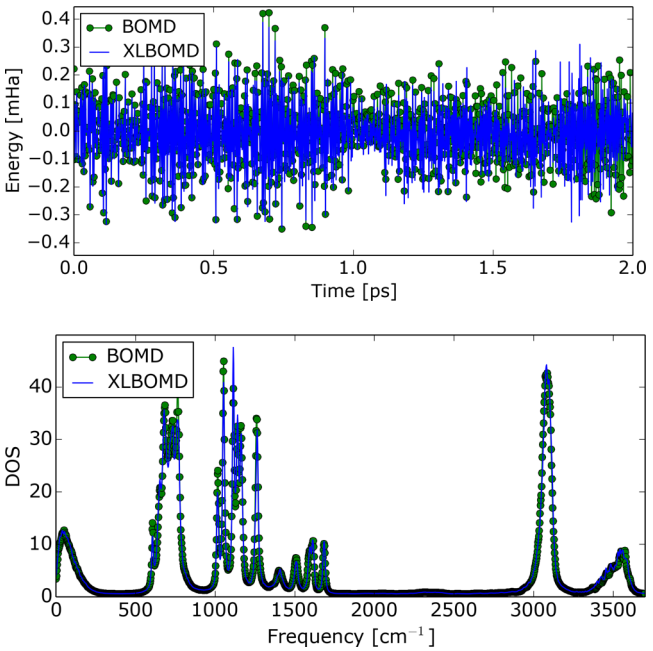

Figure 2. Total energy fluctuation (top) and vibrational density of states (bottom) for the imidazol crystal with 16 imidazol molecules using 400 K electronic and ionic temperature. Green dots and blue lines represent the results of the BOMD and XL-BOMD simulations, respectively.

give rise to long-range effects. As an example, we have investigated the performance of XL-BOMD on cubic silicon carbide (SiC). The bonds between the silicon and carbon atoms in SiC are polarized, and the amount of charge transfer between the atoms depends strongly on the interatomic distances. Therefore, this system should represent a sensitive test of whether the fast XL-BOMD formulation in the limit of only one diagonalization per time step is able to describe the physical properties of covalently bounded solids in general.

The initial geometry consisted of a 128 atom cubic (fcc) supercell. For the Brillouin-zone integration, the 2 × 2 × 2 Monkhorst–Pack k-point set[37] was used. The integration time step, δt, was chosen as 1.0 fs. The thermalization was carried out using 2000 K both for the ionic and electronic temperatures. The same electronic temperature was also applied during the following NVE dynamics. The κ-scaling parameter c for the XL-BOMD simulation was set to 0.25.

The energy fluctuations during the first 2 ps and the density of vibrational states calculated from the full trajectory are shown in Figure 3. The fluctuation of the XL-BOMD total

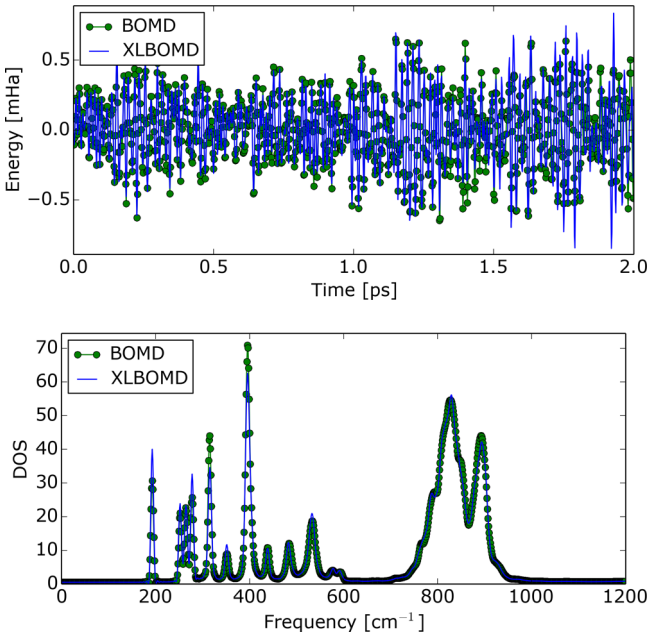

Figure 3. Total energy fluctuation (top) and vibrational density of states (bottom) for the 128 atom silicon carbide supercell at T = 2000 K. Green dots and blue lines represent the results of the BOMD and XL-BOMD simulations, respectively.

energy is again somewhat higher, as was seen for the original BOMD case. The almost identical vibrational spectra, however, confirms that the two simulations yield dynamical properties that are very close to each other.

It is interesting to note that the deviations in the energy fluctuation curves depend sensitively on the choice of the κ-scaling factor c. In the case of the SiC dynamics, a simulation with a lower value of 0.125 yielded even greater differences in the total energies, but it still gave an almost identical vibrational spectrum. This is not surprising, as the scaling factor influences the steepness of the harmonic potential in which the auxiliary charges are moving. A lower value results in a flatter potential, enabling greater deviations between the exact (fully SCC-converged) and auxiliary charges. Higher values, on the other hand, force the auxiliary charges to follow the exact charges more closely. However, in the case of SiC, setting the scaling value higher ($\geq$0.5) yielded an unstable XL-BOMD trajectory with divergent total energies already evident after a few simulation steps.

4.3. Difficult Systems. During our tests with XL-BOMD, we have identified several systems where the technique of one

DOI: 10.1021/acs.jctc.5b00324
J. Chem. Theory Comput. XXXX, XXX, XXX–XXX

diagonalization per time step results in trajectories diverging from the BOMD trajectory. One of the critical cases we have encountered was metallic Zn with a vacancy. Using a 32 atom supercell with one vacany led to diverging XL-BOMD trajectories with unphysical total energies when calculated with the `znorg-0-1` parametrization set.[38] Looking at the details of the SCC cycle reveals that the system is SCC-unstable: the total energy oscillates heavily during the subsequent SCC iterations instead of decreasing monotonically, as is usually the case. As XL-BOMD requires a convex energy functional to be stable, the instability in this case is not surprising. We have experienced similar problems with hydrogenated graphene. For pure graphene, the BOMD and XL-BOMD trajectories were almost identical. This could be expected, as the net charge transfer between the carbon atoms is small. We then investigated the dynamics of a hydrogenated graphene sheet, similar to the ones investigated in Ref. 39, where hydrogen was randomly adsorbed on 10% of the carbon atoms. The XL-BOMD simulations with one diagonalization led, in this case, to diverging total energies immediately after the start of the simulation. Similar to metallic Zn, this system is also SCC-unstable, showing strong oscillations in the total energy during the normal SCC cycle.

The obtained behavior is not really surprising. The instability is likely to be caused by the charge sloshing obtained in those extended systems. During the full SCC cycle in the BOMD simulations, the instability is damped by the applied charge mixer, yielding convergent charges at every time step and stable MD trajectories. In the limiting case of one diagonalization per time step, however, no such damping can be applied, leading to unphysical charges and diverging trajectories already after very short simulation times. We have also tested these two difficult systems by implementing and applying an inverse Jacobian kernel similar to the one described in ref 20. For the two systems tested here, however, the static inverse Jacobian kernel was not able to stabilize the trajectories.

5. SUMMARY AND CONCLUSIONS

We have presented an implementation of the extended Lagrangian Born−Oppenheimer molecular dynamics in the DFTB+ electronic structure program package for simulations of solids and molecular systems. Our approach combines the computational speed of DFTB calculations with the efficiency and long-term energy stability of extended Lagrangian Born−Oppenheimer molecular dynamics. For systems without self-consistent charge instabilities, we demonstrated how only a single diagonalization or construction of the single-particle density matrix was required in each time step with trajectories that are virtually identical to those with fully converged regular Born-Oppeheimer simulations. Our DFTB+ implementation is applicable for a broad range of materials systems, for both solids and molecules, and typically results in a speed up factor of 3−7 with respect to the speed of regular Born−Oppenheimer simulations. Systems with self-consistent charge instabilities are difficult to treat with the current formulation of fast XL-BOMD with only one diagonalization per time step. However, for such systems, one can also profit from the formalism by using its predicted charges as initial guesses for a full SCC cycle at each time step. Additionally, we are working on the generalization and implementation of the recently published generalization of the method[20] for our nonorthogonal tight-binding model, which would enable even systems with self-consistent charge instabilities to be tackled with a single diagonalization per time step.

AUTHOR INFORMATION

Corresponding Author

*E-mail: aradi@uni-bremen.de.

Funding

A.M.N.N. acknowledges support by the United States Department of Energy (U.S. DOE), Office of Basic Energy Sciences (FWP no. LANL2014E8AN).

Notes

The authors declare no competing financial interest.

ACKNOWLEDGMENTS

B.A. would like to thank C. Köhler for helpful discussions. A.M.N.N. acknowledges discussisions with M. Cawkwell, E. Chisolm, and K. Velizhanin and stimulating contributions by T. Peery at the T-Division Ten Bar Java group. LANL is operated by Los Alamos National Security, LLC, for the NNSA of the U.S. DOE under contract no. DE-AC52-06NA25396.

REFERENCES

(1) Marx, D.; Hutter, J. *Modern Methods and Algorithms of Quantum Chemistry*, 2nd ed.; Grotendorst, J., Ed.; John von Neumann Institute for Computing: Jülich, Germany, 2000.
(2) Kirchner, B.; di Dio Philipp, J.; Hutter, J. *Top. Curr. Chem.* **2012**, *307*, 109.
(3) Wang, I. S. Y.; Karplus, M. *J. Am. Chem. Soc.* **1973**, *95*, 8160.
(4) Leforestier, C. *J. Chem. Phys.* **1978**, *68*, 4406.
(5) Hohenberg, P.; Kohn, W. *Phys. Rev.* **1964**, *136*, B:864−B871.
(6) Kohn, W.; Sham, L. J. *Phys. Rev. B* **1965**, *140*, A1133.
(7) Car, R.; Parrinello, M. *Phys. Rev. Lett.* **1985**, *55*, 2471.
(8) Remler, D. K.; Madden, P. A. *Mol. Phys.* **1990**, *70*, 921.
(9) Tuckerman, M. E.; Ungar, P. J.; von Rosenvinge, T.; Klein, M. L. *J. Phys. Chem.* **1996**, *100*, 1996.
(10) Hutter, J. *Wiley Interdiscip. Rev.: Comput. Mol. Sci.* **2012**, *2*, 604.
(11) Pulay, P.; Fogarasi, G. *Chem. Phys. Lett.* **2004**, *386*, 272.
(12) Herbert, J.; Head-Gordon, M. *Phys. Chem. Chem. Phys.* **2005**, *7*, 3269.
(13) Niklasson, A. M. N.; Tymczak, C. J.; Challacombe, M. *Phys. Rev. Lett.* **2006**, *97*, 123001.
(14) Kühne, T. D.; Krack, M.; Mohamed, F. R.; Parrinello, M. *Phys. Rev. Lett.* **2007**, *98*, 066401.
(15) Niklasson, A. M. N. *Phys. Rev. Lett.* **2008**, *100*, 123004.
(16) Steneteg, P.; Abrikosov, I. A.; Weber, V.; Niklasson, A. M. N. *Phys. Rev. B* **2010**, *82*, 075110.
(17) Cawkwell, M. J.; Niklasson, A. M. N. *J. Chem. Phys.* **2012**, *137*, 134105.
(18) Lin, L.; Lu, J.; Shao, S. *Entropy* **2014**, *16*, 110.
(19) Souvatzis, P.; Niklasson, A. *J. Chem. Phys.* **2014**, *140*, 044117.
(20) Niklasson, A. M. N.; Cawkwell, M. J. *J. Chem. Phys.* **2014**, *141*, 164123.
(21) Elstner, M.; Porezag, D.; Jungnickel, G.; Elstner, J.; Haugk, M.; Frauenheim, T.; Suhai, S.; Seifert, G. *Phys. Rev. B* **1998**, *58*, 7260.
(22) Finnis, M. W.; Paxton, A. T.; Methfessel, M.; van Schilfgarde, M. *Phys. Rev. Lett.* **1998**, *81*, 5149.
(23) Frauenheim, T.; Seifert, G.; aand Z. Hajnal, M. E.; Jungnickel, G.; Porezag, D.; Suhai, S.; Scholz, R. *Phys. Status Solidi* **2000**, *217*, 41.
(24) Aradi, B.; Hourahine, B.; Frauenheim, T. *J. Phys. Chem. A* **2007**, *111*, 5678−5684.
(25) Zheng, G.; Niklasson, A. M. N.; Karplus, M. *J. Chem. Phys.* **2011**, *135*, 044122.
(26) Channel, J. P.; Scovel, C. *Nonlinearity* **1990**, *3*, 231.
(27) McLachlan, R.; Atela, P. *Nonlinearity* **1992**, *5*, 541.

DOI: 10.1021/acs.jctc.5b00324
J. Chem. Theory Comput. XXXX, XXX, XXX−XXX

(28) Niklasson, A. M. N.; Steneteg, P.; Odell, A.; Bock, N.; Challacombe, M.; Tymczak, C. J.; Holmstrom, E.; Zheng, G.; Weber, V. *J. Chem. Phys.* **2009**, *130*, 214109.
(29) Odell, A.; Delin, A.; Johansson, B.; Bock, N.; Challacombe, M.; Niklasson, A. M. N. *J. Chem. Phys.* **2009**, *131*, 244106.
(30) Leimkuhler, B.; Reich, S. *Simulating Hamiltonian Dynamics*; Cambridge University Press: Cambridge, 2004.
(31) Niklasson, A. M. N.; Cawkwell, M. J. *Phys. Rev. B* **2012**, *86*, 174308.
(32) Souvatzis, P.; Niklasson, A. *J. Chem. Phys.* **2013**, *139*, 214102.
(33) Parr, R. G.; Yang, W. *Density-Functional Theory of Atoms and Molecules*; Oxford University Press: Oxford, 1989.
(34) Dederichs, P. H.; Zeller, R. *Phys. Rev. B* **1983**, *28*, 5262.
(35) Martyna, G. J.; Tuckerman, M. E.; Tobias, D. J.; Klein, M. L. *Mol. Phys.* **1996**, *87*, 1117.
(36) Elstner, M.; Porezag, D.; Jungnickel, G.; Elsner, J.; Haugk, M.; Frauenheim, T.; Suhai, S.; Seifert, G. *Phys. Rev. B* **1998**, *58*, 7260.
(37) Monkhorst, H. J.; Pack, J. D. *Phys. Rev. B* **1976**, *13*, 5188.
(38) Moreira, H. N.; Dolgonos, G.; Aradi, B.; da Rosa, A. L.; Frauenheim, T. J. *J. Chem. Theory Comput.* **2009**, *5*, 605.
(39) Wehling, T. O.; Grundkötter-Stock, B.; Aradi, B.; Frauenheim, T.; Niehaus, T. *Phys. Rev. B* **2014**, *90*, 085422.

DOI: 10.1021/acs.jctc.5b00324
J. Chem. Theory Comput. XXXX, XXX, XXX−XXX